Inorganic Chemistry

Article

pubs.acs.org/IC

From the Ternary $Eu(Au/In)_2$ and $EuAu_4(Au/In)_2$ with Remarkable Au/In Distributions to a New Structure Type: The Gold-Rich $Eu_5Au_{16}(Au/In)_6$ Structure

Simon Steinberg,[†,‡] Nathan Card,[‡] and Anja-Verena Mudring*[,†,‡]

[†]Ames Laboratory, U.S. Department of Energy and [‡]Department of Material Sciences and Engineering, Iowa State University, Ames, Iowa 50011, United States

Supporting Information

ABSTRACT: The ternary $Eu(Au/In)_2$ ($EuAu_{0.46}In_{1.54(2)}$) (**I**), $EuAu_4(Au/In)_2$ ($EuAu_{4+x}In_{2-x}$ with x = 0.75(2) (**II**), 0.93(2), and 1.03(2)), and $Eu_5Au_{16}(Au/In)_6$ ($Eu_5Au_{17.29}In_{4.71(3)}$) (**III**) have been synthesized, and their structures were characterized by single-crystal X-ray diffraction. **I** and **II** crystallize with the $CeCu_2$-type (Pearson Symbol *oI*12; *Imma*; Z = 4; a = 4.9018(4) Å; b = 7.8237(5) Å; c = 8.4457(5) Å) and the $YbAl_4Mo_2$-type (*tI*14; *I*4/*mmm*; Z = 2; a = 7.1612(7) Å; c = 5.5268(7) Å) and exhibit significant Au/In disorder. **I** is composed of an Au/In-mixed diamond-related host lattice encapsulating Eu atoms, while the structure of **II** features ribbons of distorted, squared Au_8 prisms enclosing Eu, Au, and In atoms. Combination of these structural motifs leads to a new structure type as observed for $Eu_5Au_{16}(Au/In)_6$ ($Eu_5Au_{17.29}In_{4.71(3)}$) (*oS*108; *Cmcm*; Z = 4; a = 7.2283(4) Å; b = 9.0499(6) Å; c = 34.619(2) Å), which formally represents a one-dimensional intergrowth of the series $EuAu_2$–"$EuAu_4In_2$". The site preferences of the disordered Au/In positions in **II** were investigated for different hypothetical "$EuAu_4(Au/In)_2$" models using the projector-augmented wave method and indicate that these structures attempt to optimize the frequencies of the heteroatomic Au–In contacts. A chemical bonding analysis on two "$EuAu_5In$" and "$EuAu_4In_2$" models employed the TB-LMTO-ASA method and reveals that the subtle interplay between the local atomic environments and the bond energies determines the structural and site preferences for these systems.

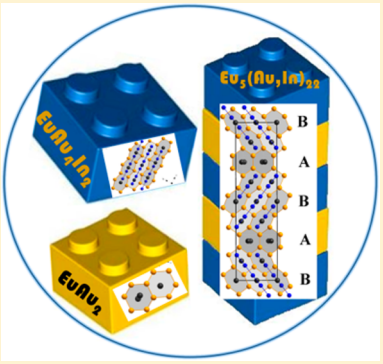

INTRODUCTION

Polar metal-rich phases with gold have created excitement among scientists because of their unusual bonding patters and rich, amazing structural chemistry, most recently the remarkable phases in the A–Au–Tr/Tt systems (A = alkaline/alkaline-earth; Tr/Tt = group 13 or 14 element).[1] The bonding patterns of these structures exhibit substantial 6s–5d orbital mixings of gold as a consequence of relativistic effects,[1−3] which have been observed for diverse more electron-poor intermetallics[4−6] as well as for quasicrystals (QCs) and their approximants (ACs).[7−11] Valence electron concentrations (vecs) and analyses of the band structures for these compounds utilizing density functional theory (DFT)-based methods place these structures between the Zintl and (close to) the Hume–Rothery phases.[5] Typically, these more electron-poor intermetallic structures feature substantial Au/Tr or Au/Tt site mixing to optimize the bonding for the polyanionic networks, but still, the homogeneity ranges for these structures indicate certain electronic flexibilities.[12]

One class of compounds is the broad family of structures with diamond-like gold networks, which are observed for five different structure types: the rhombohedral $Sr_2Au_{6+x}Zn_{3-x}$-type (*R*-3*c*),[13] the hexagonal $SrAu_{4+x}Al_{3-x}$-type (*P*-62*m*),[14] two independent orthorhombic structures, i.e. $SrAu_{5+x}Al_{2-x}$-[14] and $BaAu_5Ga_2$-type (*Pnma*, both structures),[15] and the monoclinic $Sr_2Au_{6+x}Zn_{3-x}$-type (*C*2/*c*).[13] The voids within the Au host frameworks encompass triangular $[Au,M]_3$ clusters (M = Al, Zn, Ga, In, or Sn) or alkaline-earth Ae (Sr, Ba) and Eu atoms,[13−18] which are mutually exchanged for particular $SrAu_{4+x}Al_{3-x}$-type structures. All these structures can be derived from the binary AAu_2 (A = Sr, Ba, Eu)[19−21] to the extent that they are components of the Fibonacci series $(Au_{12/6}A)_m(Au_{12/6}M_3)_n$ (A = Sr, Ba, Eu) with AAu_2 for m = 1, n = 0, AAu_4M_3 for m = 1, n = 1, $A_2Au_6M_3$ for m = 2, n = 1, and $Ba_{1.04}Au_{4.5}Ga_{2.4}$ or $Eu_{1.1}Au_{4.4}Ga_{2.2}$ for m = 3 and n = 2.[15]

Another class of Au-rich intermetallic compounds which show certain electronic flexibilities comprises those structures adopting the $YbAl_4Mo_2$-type.[22−26] This type of structure is composed of an aluminum network encapsulating ytterbium and molybdenum atoms, respectively.[24] While previous examinations concentrated primarily on the A–Au–Tr/Tt systems, the Au-rich parts of the R–Au–Tr/Tt phase diagrams (R = rare-earth element) have been studied to a lesser extent.[27−29] Initial hints of rare-earth-containing $SrAu_{4+x}Al_{3-x}$-[15] and $Sr_2Au_{6+x}Zn_{3-x}$-type[18] compounds draw our interest to unprecedented realms of Au-rich, polar intermetallic compounds in the *R*–Au–Tr/Tt phase diagrams. Despite the fact that more recent research on the Eu–Au–In system has focused on its In-rich region,[30−32] still, there are

Received: February 3, 2015
Published: August 13, 2015

DOI: 10.1021/acs.inorgchem.5b00257
Inorg. Chem. 2015, 54, 8187–8196

Table 1. Details of the Crystal Structure Investigations and Refinements for $EuAu_{0.5}In_{1.5}$, $EuAu_{4.8}In_{1.2}$, and $Eu_5Au_{17.3}In_{4.7}$

	$EuAu_{0.46}In_{1.54(2)}$ (I)	$EuAu_{4.75}In_{1.25(2)}$ (II)	$Eu_5Au_{17.29}In_{4.71(3)}$ (III)
fw	419.80	1231.08	4705.95
space group	*Imma* (No. 74)	*I*4/*mmm* (No. 139)	*Cmcm* (No. 63)
a, Å	4.9018(4)	7.1612(7)	7.2283(4)
b, Å	7.8237(5)		9.0499(6)
c, Å	8.4457(5)	5.5268(7)	34.619(2)
vol., Å^3	323.89(4)	283.43(7)	2264.6(2)
Z	4	2	4
density (calcd), g/cm^3	8.609	14.425	13.803
μ, mm^{-1}	50.65	138.17	129.74
F(000)	700	999	7646
θ range	3.6−33.0	4.7−32.7	5.6−28.0
index ranges	$-8 \le h \le 9$	$-6 \le h \le 12$	$-8 \le h \le 8$
	$-14 \le k \le 14$	$-11 \le k \le 11$	$-11 \le k \le 11$
	$-14 \le l \le 15$	$-9 \le l \le 9$	$-42 \le l \le 42$
no. of reflns collected	3617	2054	10702
no. of independent reflns/R_{int}	596/0.066	238/0.068	1233/0.154
no. of reflns with $I > 2\sigma(I)/R_\sigma$	456/0.043	196/0.035	792/0.084
refinement method		full-matrix least-squares on F^2	
data/restraints/parameter	596/0/13	238/0/11	1233/0/77
goodness-of-fit on F^2	1.04	1.11	1.01
final *R* indices [$F^2 > 2\sigma(F^2)$]	$R_1 = 0.035$; $wR_2 = 0.069$	$R_1 = 0.026$; $wR_2 = 0.049$	$R_1 = 0.044$; $wR_2 = 0.075$
R indices (all data)	$R_1 = 0.053$; $wR_2 = 0.077$	$R_1 = 0.035$; $wR_2 = 0.051$	$R_1 = 0.086$; $wR_2 = 0.090$
largest diff. peak and hole, e$^-$/Å^3	5.12 and −4.16	2.55 and −2.30	4.59 and −3.89

barely any reports regarding its Au-rich (more electron-poor) part.[33] Therefore, we present and discuss the results of the initial explorations for the Au-rich part of the Eu−Au−In system, which yielded the intermetallic compounds $EuAu_{0.5}In_{1.5}$, $EuAu_{4+x}In_{2-x}$ (x = 0.8−1.0), and $Eu_5Au_{17.3}In_{4.7}$ with a new structure type for the last composition.

EXPERIMENTAL TECHNIQUES

Syntheses. Gold pieces (99.999%, BASF), filings of europium (99.99%, Ames Laboratory), indium and gallium ingots (99.999% Alfa Aesar) were used as starting materials and stored and handled under dry argon atmosphere in a glovebox (H_2O < 0.1 ppmv). The Eu filings were produced from large ingots, which were mechanically polished prior to each use. Loads of ∼200−300 mg total were weighed in precleaned, one-side arc-welded tantalum tubes, which were closed inside a glovebox, arc welded on the other end, and jacketed by evacuated Schlenk flasks. The products were obtained using the following temperature programs. $EuAu_{0.5}In_{1.5}$: heat to 800 °C within 4 h, keep that temperature for 12 h, cool to 300 °C with 10 °C/h, and anneal at this temperature for 60 h. $EuAu_{4+x}In_{2-x}$ (x = 0.8) and $Eu_5Au_{17.3}In_{4.7}$: heat to 800 °C in 4 h, keep the temperature for 12 h, slowly cool to 300 °C (2 °C/h), anneal at this temperature for 3 days, and quench in water. Single crystals obtained from samples with loads corresponding to hypothetical compositions of "$Eu_2Au_7In_2$" and "$Eu_1Au_5In_1$" (Supporting Information; Table S1) pointed to a narrow solid solution for $EuAu_{4+x}In_{2-x}$ (x = 0.8−1.0). The products appeared as gray powders with silver crystals of polyhedral shapes and metallic luster and were stable in air in accord with recently reported Au-rich compounds.[15,16] Analogous reactions in the Eu−Au−Ga system yielded a rhombohedral $Sr_2Au_{6+x}Zn_{3-x}$-type[13] phase ($Eu_2Au_{6.1}Ga_{2.9}$; *R*-3*c*; a = 8.411(5) Å; c = 21.830(13) Å, see Supporting Information) or hexagonal $SrAu_{4+x}Al_{3-x}$-type[14] compounds, which have been reported elsewhere.[15]

X-ray Studies. All samples were checked for purity through detailed phase analyses of sets of powder X-ray diffraction data, which were collected on STOE STADI P diffractometers equipped with a STOE image plate and DECTRIS MYTHEN 1K detectors (Cu $K_{\alpha 1}$; λ = 1.54059 Å) at room temperature. For the measurement the samples were dispersed on Mylar sheets with grease and placed between split aluminum rings or sealed in capillaries. Data and phase analyses were carried out with the *WinXPow* software package.[34] Detailed phase analyses of the powder patterns revealed that $EuAu_{4+x}In_{2-x}$ (x = 0.75(2) (**II**), 0.93(2), and 1.03(2)) were obtained as high-yield products in competition with $Eu_5Au_{17.3}In_{4.7}$ (**III**), while $EuAu_{0.5}In_{1.5}$ (**I**) was accompanied by the previously reported EuAuIn[35] (see Supporting Information).

Single crystals were selected from the bulk samples, fixed on glass fibers with grease, and subsequently transferred to a Bruker APEX CCD diffractometer (Bruker, Inc.; Madison, WI). Sets of single-crystal X-ray intensity data were collected in φ- and ω-scan modes at room temperature (∼296 K) with Mo Kα radiation (λ = 0.71073 Å) and exposures of 15 s/frame. The raw intensity data were integrated utilizing the *SAINT* program within the *SMART* software suite,[36] while the program *SADABS*[37] was employed for empirical absorption corrections.

Checking the intensity data sets for extinction conditions with the *XPREP* algorithms in the *SHELXTL* suite[38] and examination of the E^2-1 statistics lead to the assignment of the centrosymmetric space groups *Imma* (No. 74), *I*4/*mmm* (No. 139), and *Cmcm* (No. 63) for $EuAu_{0.46}In_{1.54(2)}$ (**I**), $EuAu_{4+x}In_{2-x}$ (x = 0.75(2) (**II**), 0.93(2), and 1.03(2)), and $Eu_5Au_{17.29}In_{4.71(3)}$ (**III**), respectively. All structures were solved using direct methods (*SHELXS-2013*) and refined on F^2 in full-matrix least-squares including anisotropic atomic displacement parameters (*SHELXL-2013*).[39] Initial refinements of the 8*h* sites in **I** and the 4*d* positions in **II** with the scattering factor of indium lead to too small displacement parameters for these sites, and close inspection of the Fourier maps for **I** and **II** indicated higher electron densities on these sites; however, subsequent refinements with the scattering factors of gold resulted in too large anisotropic atomic displacement parameters for the 8*h* sites in **I** and the 4*d* positions in **II**. Accordingly, mixed Au/In occupancies were introduced for these sites, and approaches to refine them with the same as well as different positional parameters for both gold and indium preceded to more reasonable anisotropic atomic displacement parameters for the refinements with the common Au/In positions. Analogous examinations of the 16*h* and 8*f* positions for the orthorhombic structure of **III** indicated the presence of mixed Au/In occupancies for the latter sites. Therefore, mixed Au/In occupancies were assigned on three 8*f* positions in the structure of **III**, which was refined to the composition

DOI: 10.1021/acs.inorgchem.5b00257
Inorg. Chem. 2015, 54, 8187−8196

Table 2. Atomic Positions and Equivalent Isotropic Displacement Parameters for $EuAu_{0.46}In_{1.54(2)}$, $EuAu_{4.75}In_{1.25(2)}$, and $Eu_5Au_{17.29}In_{4.71(3)}$

atom	position	x	y	z	U_{iso}/U_{eq}, Å^2	Occ. (<1)
			$EuAu_{0.46}In_{1.54(2)}$			
Eu1	4*e*	0	1/4	0.5418(1)	0.0170(2)	
Au2/In2	8*h*	0	0.0485(1)	0.1637(1)	0.0181(2)	0.23(1)/0.77(1)
			$EuAu_{4.75}In_{1.25(2)}$			
Au1	8*h*	0.3059(1)	0.3059(1)	0	0.0129(2)	
Eu2	2*a*	0	0	0	0.0112(3)	
Au3/In3	4*d*	0	1/2	1/4	0.0156(4)	0.37(1)/0.63(1)
			$Eu_5Au_{17.29}In_{4.71(3)}$			
Au1	16*h*	0.1933(2)	0.3090(1)	0.4620(1)	0.0108(3)	
Au2	16*h*	0.1975(2)	0.4228(1)	0.2901(1)	0.0089(3)	
Au3	16*h*	0.1931(2)	0.0630(1)	0.4136(1)	0.0108(3)	
Au4	16*h*	0.3064(2)	0.1765(1)	0.3367(1)	0.0115(3)	
Au5/In5	8*f*	0	0.4057(3)	0.5319(1)	0.0085(10)	0.20(2)/0.80(2)
Au6/In6	8*f*	1/2	0.2846(3)	0.4045(1)	0.0119(11)	0.37(2)/0.63(2)
Au7/In7	8*f*	1/2	0.4833(4)	0.3395(1)	0.0165(14)	0.07(2)/0.93(2)
Eu8	4*a*	1/2	1/2	1/2	0.0091(7)	
Eu9	8*f*	0	0.3703(3)	0.3755(1)	0.0093(6)	
Eu10	4*c*	0	0.7087(4)	1/4	0.0065(7)	
Eu11	4*c*	0	0.1472(4)	1/4	0.0101(8)	

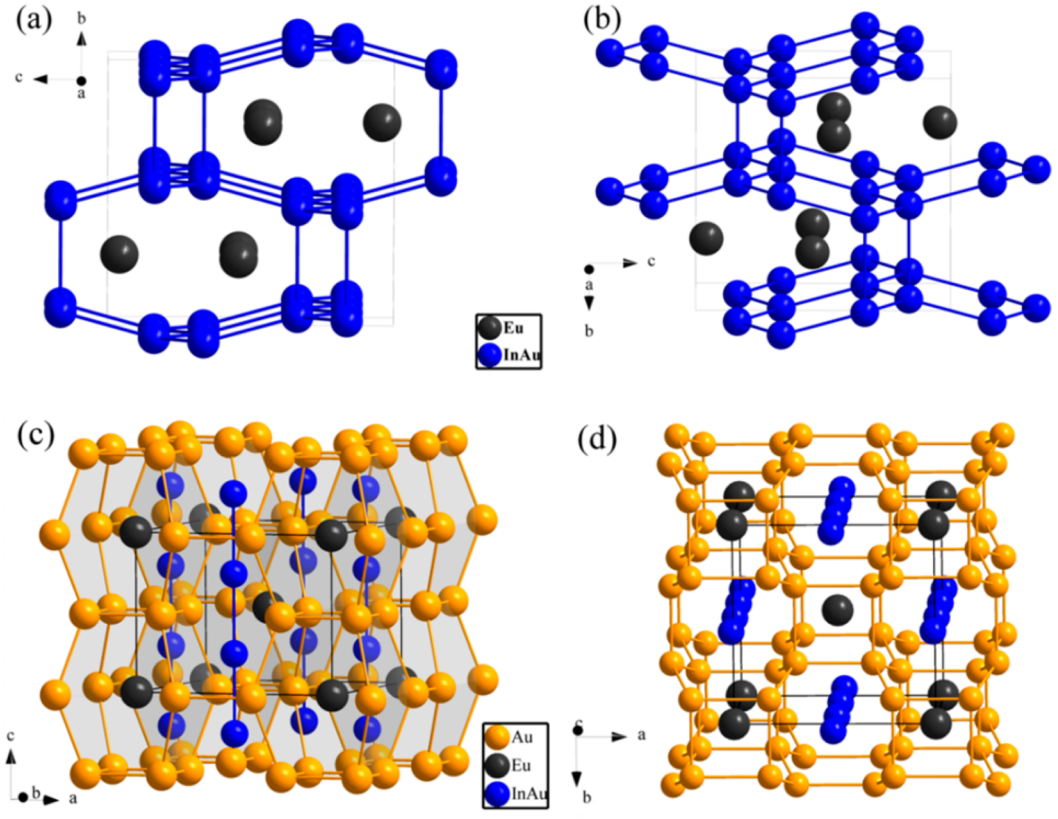

Figure 1. Representation (a) of the unit cell of **I**: Au and In atoms form hexagons in chair conformations within the *ac* plane (b). (c) View on the unit cell of **II**: each europium atom is enclosed by 12 Au and 8 M atoms, while the gold network may be depicted as mutually perpendicular gold hexagons in boot conformations (d).

$Eu_5Au_{17.29}In_{4.71(3)}$ for the selected single crystal. The *PLATON* software package[40] was employed to check the symmetries of the refined structures, and no higher symmetries were identified. With these settings the R_1 values converged to less than 4.36% (Table 1). Details of the data collection and refinement parameters for **I**, **II**, and **III** are provided in Table 1, whereas atomic positions are listed in Table 2.

Computational Details. Electronic structure calculations were undertaken for hypothetical $EuAu_4(Au/In)_2$ (**II**) models representing the compositions "$EuAu_4In_2$" and "$EuAu_5In$" (Figure 3) to identify the site preferences in the tetragonal structures. The "$EuAu_4In_2$" model differs from the experimentally determined tetragonal $EuAu_{4+x}In_{2-x}$ structures (x = 0.8−1.0) through full indium occupation of the 4*d* site, while in the "$EuAu_5In$" models indium atoms reside on both the 8*h* and 4*d* sites. Full structural optimizations of all models and band

DOI: 10.1021/acs.inorgchem.5b00257
Inorg. Chem. 2015, 54, 8187−8196

structure calculations were carried out using the projector-augmented wave (PAW) method of Blöchl[41] as implanted in the *Vienna ab initio Simulation Package* (VASP) by Kresse and Joubert.[42−46] Correlation and exchange were described by the general gradient approximation of Perdew, Burke, and Enzerhof (GGA−PBE),[47] while starting meshes of 4 × 4 × 4 up to 8 × 8 × 8 *k* points were employed to sample the first Brillouin zone for reciprocal space integrations. The cutoff energy of the plane wave basis sets was set 500 eV, and full optimizations were accomplished until the energy difference between two iterative steps fell below 10^{-7} eV/cell. An effective on-site Coulomb interaction term (U_{eff} = 3 eV) was included in the Kohn−Sham Hamiltonian to account for the strong correlations within the Eu 4*f* states.

A chemical bonding analysis on all models was completed based on the integrated values of the crystal orbital Hamilton populations (COHP), which were obtained through the tight-binding linear-muffin-tin-orbital (TB-LMTO) method with the atomic sphere approximation (ASA) using the Stuttgart code.[48,49] In particular, the off-site projected density of states are weighted by the corresponding Hamilton matrix elements to determine bonding and antibonding states.[50] The optimized structural parameters of the models were obtained from the VASP computations and used as starting points for the TB-LMTO-based electronic structure calculations. The Wigner−Seitz (WS) radii were generated automatically, and empty spheres (ES) were included to achieve an optimal approximation of full potentials. The basis set employed the following orbitals (down-folded[51] orbitals in parentheses): Au-6s/-6p/-5d/(-5f); Eu-6s/(-6p)/-5d; In-5s/-5p/(-5d)/(-4f). The corresponding WS radii (Angstroms) were as follows: Au, 2.91−3.13; Eu 3.49−3.72; In, 3.02−3.14. On the basis of the VASP computations the Eu 4*f* states are strongly localized and, hence, treated as core-like states in the TB-LMTO-based calculations, which is in accord with recently reported results on *R*-containing compounds.[52−54] Reciprocal space integrations were completed with the tetrahedron method[55] employing 24 × 24 × 24, 24 × 24 × 24, 24 × 24 × 24, 12 × 6 × 12, and 12 × 12 × 6 *k*-point sets for the "$EuAu_4In_2$", "$EuAu_5In$-1", "$EuAu_5In$-2", "$EuAu_5In$-3", and "$EuAu_5In$-4" models, respectively. Plots of the DOS and −COHP curves are shown in Figure 4, while the integrated values of the −COHP curves (ICOHP) may be extracted from the Supporting Information (Tables S3−S6).

RESULTS AND DISCUSSION

More recent investigations of the Au-rich part of the Eu−Au−Tr (Tr = Al, Ga) systems have resulted in the identification of rhombohedral $Sr_2Au_{6+x}Zn_{3-x}$-type[13,18] (Table S1, Supporting Information) or hexagonal $SrAu_{4+x}Al_{3-x}$-type[14,15] compounds. Initial examinations of the Eu-poor regions (<33 at.%) for the corresponding Eu−Au−In system lead to the discovery of the Au-rich $EuAu_{4+x}In_{2-x}$ (x = 0.75(2) (**II**)) and $Eu_5Au_{17.29}In_{4.71(3)}$ (**III**), which were detected at the same composition "$Eu_2Au_7In_2$". Furthermore, the ternary $EuAu_{0.46}In_{1.54(2)}$ (**I**) was also found at this composition. Subsequent reactions of samples loaded as "$EuAu_5In$" produced high yields of $EuAu_{4+x}In_{2-x}$ (x = 0.8−1.0; Figure S3, Supporting Information), while loadings of "$EuAu_4In_2$" uncovered the possibility of Tsai-type quasicrystals and their approximants in this system.

Crystal Structures. The structure of $EuAu_{0.46}In_{1.54(2)}$ (**I**) is derived from the binary $EuAu_2$ (*Imma*; No. 74; $CeCu_2$-type[56]) through partial indium substitution on the gold sites (Wyckoff position 8*h*).[21] In particular, this structure features puckered sheets of gold/indium-mixed (M) hexagons adopting chairlike conformations within the *ac* plane. The M−M distances are short (2.851(1)−2.868(1) Å) within the M_6 rings and range from 3.152(1) to 4.671(1) Å between the M hexagons sandwiching the Eu host atoms (Wyckoff position 4*e*). Accordingly, each europium atom is enclosed by 12 M atoms forming condensed Eu@$M_{12/6}$ cages (Figure 1). Note that the structure of **I** crystallizes with the $CeCu_2$-[56] rather than the $CaIn_2$-type ($P6_3/mmc$; No. 194), which is adopted by the binary $EuIn_2$.[57] Alike Au/In distributions have also been observed for the polyanionic networks of the previously reported $BaAu_{0.4}In_{1.6}$[58] and $GdAu_{0.4}In_{1.6}$.[59] The structure of the barium-containing compound represents a substitutional solution of gold in $BaIn_2$[60] ($CeCu_2$-type[56]), while the M network of $GdAu_{0.4}In_{1.6}$ ($CaIn_2$-type[57]) assembles a hexagonal diamond-like substructure as observed for the rhombohedral $Eu_2Au_{6.1}Ga_{2.9}$ (see Supporting Information).

Alloys in the series $EuAu_{4+x}In_{2-x}$ (x = 0.8−1.0) adopt the $YbAl_4Mo_2$-type of structure (*I*4/*mmm*; No. 139)[24] and are composed of gold networks encapsulating Eu and M (M = Au/In) atoms, respectively. The structures of the $EuAu_{4+x}In_{2-x}$ (x = 0.8−1.0) series show alike structural features, and the indium-richest representative, $EuAu_{4.75}In_{1.25(2)}$, was selected for further structural analysis. Gold atoms residing on Wyckoff position 8*h* form mutually perpendicular, puckered layers of Au_6 hexagons, which adopt boot-like conformations within the *ac* and *bc* planes (Figure 1). The Au−Au distances along the apexes of the hexagons (2.986(1) Å) are longer than the Au−Au separations (2.780(1) Å) that encompass the bases of the Au_6 circles and, furthermore, the Au_4 squares parallel to the *ab* plane. Alternatively, the Au substructure can be depicted as distorted, squared Au_8 prisms that are condensed via common faces to construct ribbons along (001). Each europium atom (Wyckoff position 2*a*) is enclosed by two face-sharing Au_8 prisms with eight M atoms (Wyckoff position 4*d*) capping their faces along the *c* axis (Figure S5, Supporting Information). Accordingly, each europium atom is coordinated by 12 Au and eight M atoms, guiding to a coordination number of 20 for Eu. Similarly, each M atom occupies a center of a distorted, squared Au_8 prisms with Au−M distances of 2.939(1) Å. Additionally, the M@Au_8 cages are bicapped by the endohedral M atoms of the nearest neighboring Au_8 prisms leading to M−M contacts of 2.763(1) Å within the ribbons.

The nearest structural analogues come from the previously reported $SrAu_{4.8}In_{1.2}$[25] and $EuAu_{4.8}Cd_{1.2}$[26] ($YbAl_4Mo_2$-type;[24] both structures). The Sr-containing structure features close M−M contacts (M = Au/In; 2.764(1) Å) within the chains and Au−Au distances of 2.782(1) Å for the Au_4 squares, while the M−M distances (here M = Au/Cd) are 2.730(1) Å within the chains in the structure of $EuAu_{4.8}Cd_{1.2}$. A clear difference between $SrAu_{4.8}In_{1.2}$ and the structures of $EuAu_{4+x}In_{2-x}$ (x = 0.93(2), 1.03(2); Supporting Information) arises from the distribution of the Au and In atoms, as the mixed 4*d* sites are occupied by about or even more than 50 atom % Au in the Eu-containing compounds. Comparatively, phase analytical studies based on powder X-ray diffraction data for the Eu−Au−Cd systems pointed to a substitutional homogeneity range of $0 \le x \le 1$ for $EuAu_{4+x}Cd_{2-x}$;[26] yet, a "$EuAu_4In_2$" composition, which shows no Au/In mixing for the 4*d* sites, has not been observed for this system. Previous investigations in the Ce−Mn−Cu[61] and La−Ag−Mg[62] systems indicated that the ranges of compositions for solid solutions with the $YbAl_4Mo_2$ type of structure partially overlap with those of different structure types. For instance, an increase of the Ag content in $LaAg_{4+x}Mg_{2-x}$ going from x = 0.4 to x = 0.9 leads to a different chemical occupation of the relative crystallographic sites and an order−disorder transformation from the $YbAl_4Mo_2$- (*I*4/*mmm*; No. 139) to the $LaAg_5Mg$-type (*P*4/*nmm*; No. 129).[62] Such polymorphism could not be encountered for the structures of $EuAu_{4+x}In_{2-x}$ (x = 0.8−1.0), as close inspection of the extinction conditions for the X-ray

DOI: 10.1021/acs.inorgchem.5b00257
Inorg. Chem. 2015, 54, 8187−8196

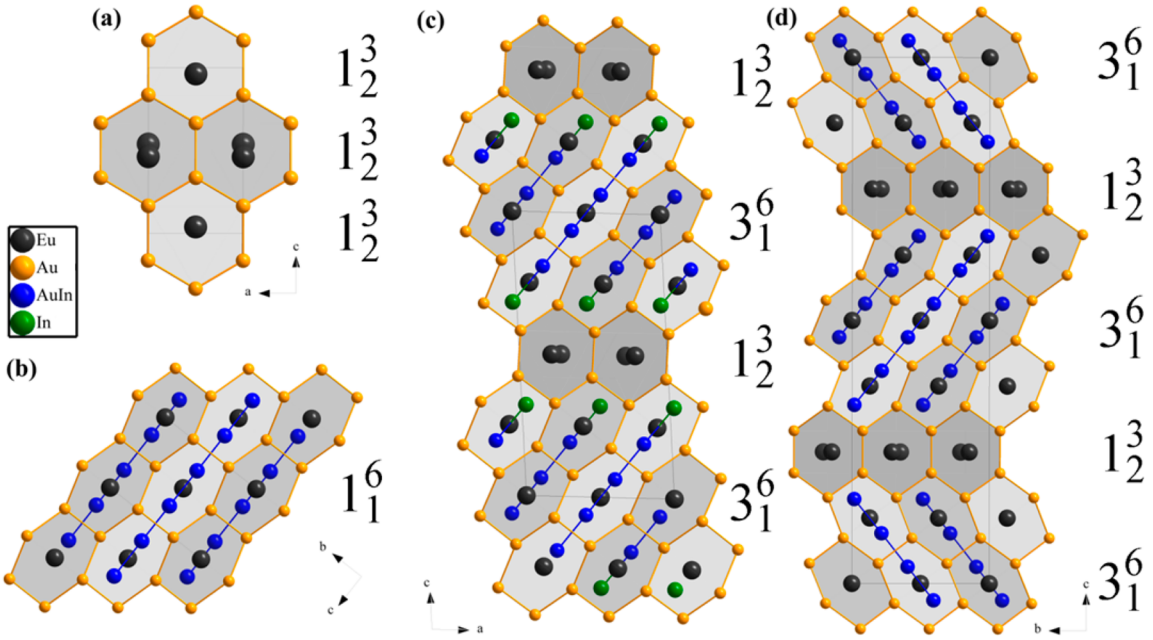

Figure 2. Representatives of the linear, inhomogeneous intergrowth series $EuAu_2$[21] (1_2^3; a)–"$EuAu_{4+x}In_{2-x}$" (1_1^6; b; Eu, dark gray; Au, yellow; M, blue; In, green): the monoclinic $Eu_5Au_{17.7}In_{4.3}$[33] (*C*2/*m*; c) and orthorhombic $Eu_5Au_{17.3}In_{4.7}$ (*Cmcm*; d) formally represent one-dimensional intergrowths of the series $EuAu_2$–"$EuAu_{4+x}In_{2-x}$". Full indium occupations of the disordered 4*d*, 4*i*, and 8*f* sites for $EuAu_{4.8}In_{1.2}$, $Eu_5Au_{17.7}In_{4.3}$, and $Eu_5Au_{17.3}In_{4.7}$, respectively, lead to the compositions "$EuAu_4In_2$" and "$Eu_5Au_{16}In_6$", which point to the presence of an intergrowth series. The two-dimensional parent segments $EuAu_2$ and "$EuAu_{4+x}In_{2-x}$" form infinite slabs stacked along (001) for both intergrowths. Note the dissimilar stacking between the monoclinic (c) and the orthorhombic (d) structures.

intensity data sets as well as E^2-1 statistics for these structures clearly pointed to the space group *I*4/*mmm*. It is worth noting that mixed occupancies occur on the 4*d* rather than the 8*h* sites in the crystal structures of the $YbAl_4Mo_2$-type ternary phases with substitutional homogeneity ranges;[25,26,61−63] however, conclusive hints accounting for this preference have not been provided. Electronic structure calculations on different "$EuAu_5In$" models will provide insight into the origin for this site preference (see Coloring and Electronic Structure).

$Eu_5Au_{17.29}In_{4.71(3)}$ (**III**) crystallizes in its own structure type (*Cmcm*; No. 63) and formally resembles a one-dimensional (or linear) intergrowth of "$EuAu_{4+x}In_{2-x}$"-related (the term "$EuAu_{4+x}In_{2-x}$" refers to segments showing the similar structural features as observed for $EuAu_{4+x}In_{2-x}$ (x = 0.8 −1.0)) and $EuAu_2$-related (two-dimensional) slabs. Strictly speaking, evaluation of a direct structural relationship between $EuAu_{4.75}In_{1.25(2)}$ and $Eu_5Au_{17.29}In_{4.71(3)}$ is set hurdles by the dissimilar occupancies of the disordered positions in **II** and **III**; however, a topological analysis of all structures with an approximation of full indium occupancies for the mixed Au/In 4*d* and 8*f* positions in **II** and **III**, respectively, guides to a structural relationship akin to a linear inhomogeneous intergrowth from $EuAu_2$ and **II** to **III**.

The orthorhombic structure contains three independent M sites (Wyckoff positions 8*f*, 8*f*, 8*f*) residing in the centers of the distorted, squared Au_8 prisms. The contacts between two endohedral M atoms (2.790(4)−2.879(4) Å) are slightly larger than those observed for **II** and suggest coordination environments of eight Au and two M atoms for the four M atoms within one ribbon (Figure S6, Supporting Information); however, the M@Au_8 cages at the ends of each ribbon are capped by one M and one Eu atom (d(Eu−M) = 3.436(4) Å). In addition to the intercalation of the $EuAu_2$-fashioned slabs, the orthorhombic structure comprises four independent europium positions. Two europium sites (Wyckoff positions 4*c*, 4*c*) are located in the Au_{12} cages of the $EuAu_2$ segments, whereas two other europium sites (Wyckoff position 4*a* and 8*f*) are enclosed by face-sharing Au_8 prisms (Figure S6, Supporting Information). The Eu atoms in the centers of the "$EuAu_{4+x}In_{2-x}$"-related slabs (Wyckoff position 4*a*) are surrounded by 12 Au and eight M atoms in accord with the Eu coordination spheres in **II**, while the europium atoms residing on Wyckoff position 8*f* possess (12Au + 7M) coordination environments. In contrast to the tetragonal structure the bases of the Au_8 prisms show slight distortions, as they range from 2.785(2) to 2.794(2) Å within and from 2.799(2) to 2.856(2) Å at the edges of the "$EuAu_{4+x}In_{2-x}$" segments. The Au−Au contacts in and between the Au_6 rings of the $EuAu_2$ layers scale from 2.776(2) to 2.861(2) Å, in fair agreement with those observed for $EuAu_2$[21] (2.714−2.917 Å).

The nearest structural analogue comes from the previously reported $Eu_5Au_{17.7}In_{4.3}$ (*C*2/*m*; No. 12),[33] which is also composed of $EuAu_2$- and "$EuAu_{4+x}In_{2-x}$" parental segments. Although a strict structural comparison between **II**, **III**, and the monoclinic structure cannot be accomplished due to the dissimilar disorder of the M positions, a topological analysis of the segments for $Eu_5Au_{17.3}In_{4.7}$ and $Eu_5Au_{17.7}In_{4.3}$ implies that these structures resemble one-dimensional (or linear) intergrowths in the series $EuAu_2$–"$EuAu_{4+x}In_{2-x}$" based on the approximations of full indium occupancies for the disordered M sites in these structures. In particular, the orthorhombic $Eu_5Au_{17.3}In_{4.7}$ and the monoclinic $Eu_5Au_{17.7}In_{4.3}$ both feature sequences of three succeeding "$EuAu_{4+x}In_{2-x}$" segments (3_1^6) and one $EuAu_2$ slab (1_2^3), which are stacked alternately along (001) in accordance with the formulas $(3_1^6 1_2^3)$ and $(3_1^6 1_2^3)_2$ for the monoclinic and orthorhombic structures, respectively (Figure 2). The superscript indexes 3 and 6 represent mirror planes and two-folded axes, respectively, that are arranged

DOI: 10.1021/acs.inorgchem.5b00257
Inorg. Chem. 2015, 54, 8187−8196

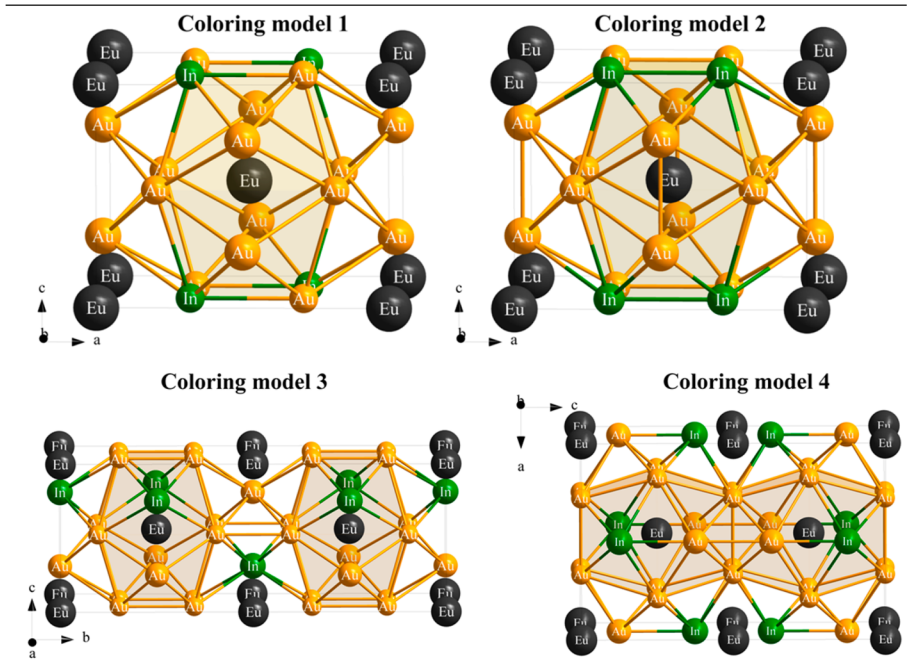

Model number	Number of homoatomic *M*–*M* contacts	Number of heteroatomic Au–In contacts	Percentage contribution of the Au–In bonds to all *M*–*M* contacts	Total energy/f.u. (eV)
1	36	16	30.77	−23.892478
2	38	14	26.92	−23.903980
3	64	40	38.46	−24.530155
4	68	36	34.61	−24.346941

Figure 3. Coloring models of hypothetical "$EuAu_5In$" structures: gold and indium sites are represented by the gold and green atoms, respectively. In models 1 and 2 (top) the indium atoms reside on the 8*h* sites, while the 4*d* positions are occupied by indium in models 3 and 4 (bottom). From the total energies of the different schemes it is clear that there is a site preference for the 4*d* sites. Placing In on the 4*d* sites surrounded by 10 nearest neighboring gold atoms leads to the maximum possible number of 10 heteroatomic Au–In contacts per In. Because each model comprises 26 M–M contacts/fu, the maximal percentage of the Au–In bonds to all M–M contacts is reached for 38.46%, which is achieved for "$EuAu_5In$-3". Models 3 and 4 are constructed of two "$EuAu_{4+x}In_{2-x}$" segments to accomplish broader options for structural variations.

perpendicular to the stacking direction within one segment.[64] In the orthorhombic structure the neighboring layers of the three succeeding "$EuAu_{4+x}In_{2-x}$" parental segments (3_1^6) are aligned in opposite directions with a torsion angle of 102.7°, while the "$EuAu_{4+x}In_{2-x}$" slabs line up in the same direction in the monoclinic structure (Figure 2). Accordingly, the orthorhombic structure comprises two ($3_1^6 1_2^3$) sections in succession and has a longer translation period along the stacking direction than the monoclinic compound. The disordered M sites of the orthorhombic structure exhibit larger indium contributions relative to the monoclinic compound and lead to a higher indium content in **III** than for the monoclinic $Eu_5Au_{17.7}In_{4.3}$.

Coloring and Electronic Structure. An analysis of the electronic structure for the ribbons of the face-sharing Au_8 cages enclosing Eu, Au, and In atoms was accomplished for the tetragonal structures, which show the shortest repeat unit along (001) within the series $EuAu_{4.8}In_{1.2}$, $Eu_5Au_{17.7}In_{4.3}$, and $Eu_5Au_{17.3}In_{4.7}$. To understand the site preference for the mixed Au/In occupancy on the Wyckoff position 4*d* different starting models were examined (see Computational Details): an ordered "$EuAu_4In_2$" model that is derived from the tetragonal structures through full indium occupations of the mixed M sites and diverse "$EuAu_5In$" models with mixed Au/In occupations on both the 8*h* (models 1 and 2) and the 4*d* (models 3 and 4) sites, respectively (Figure 3). The diverse "$EuAu_5In$" models were inspected to reveal the influence of dissimilar heteroatomic Au–In bond frequencies and different local atomic environments on the arrangements of gold and indium in the tetragonal structures. In intermetallic compounds with disordered networks the model with the maximal number of heteroatomic contacts tends to provide the lowest total energy and is typically expected to be the most favorable scheme to compare to the experimental structure.[65−67] To examine a likely presence of this tendency for the tetragonal compounds, schemes with maximal numbers of heteroatomic Au–In contacts have been achieved for the gold and indium distributions in models 1 and 3, which resemble Au/In partitioning on the 8*h* and 4*d* sites of the observed structure, respectively. The Au/In distributions in "$EuAu_5In$" models 2 and 4 give slightly lower amounts of Au–In contacts relative to "$EuAu_5In$-1 and -3", respectively, to develop tendencies between the bond frequencies, local atomic environments, and bond as well as total energies for this series. The outcome of this analysis will help to understand the site preferences for this particular system and to corroborate the experimentally determined structure as the electronically most favorable.

A topological analysis of the tetragonal structure reveals that an indium occupation of the 8*h* site brings about a maximum of 8 heteroatomic Au–In contacts per indium atom, while placing

DOI: 10.1021/acs.inorgchem.5b00257
Inorg. Chem. 2015, 54, 8187−8196

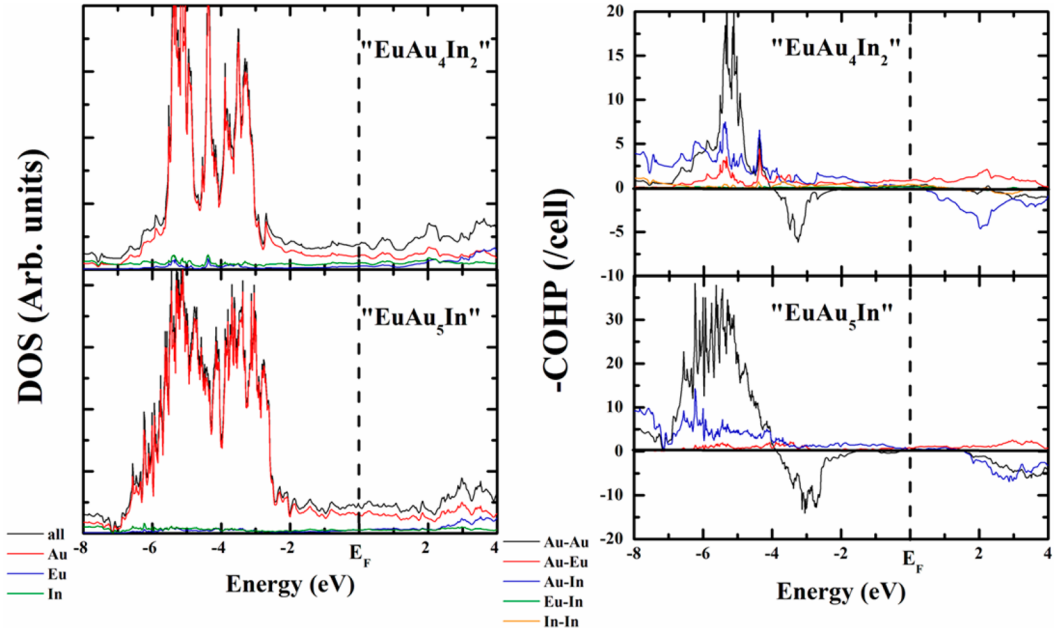

Figure 4. DOS (left) and −COHP curves (right) of the "$EuAu_4In_2$" and "$EuAu_5In$" models computed by the TB-LMTO method: the Fermi level is represented by the dashed lines, while orbital-projected DOS curves of both models may be extracted from the Supporting Information (Figure S9). Optimized structural parameters of the "$EuAu_5In$" model 3, which is the "$EuAu_5In$" composition with the lowest total energy, were used as starting points for the TB-LMTO-based calculations. Spin-polarized DOS curves (VASP) are provided in Figure S8, Supporting Information.

indium on the Wyckoff position 4*d* leads to a maximum of 10 Au−In contacts/In. Accordingly, higher Au−In bond frequencies are achieved for all M−M contacts in models 3 and 4, in which the indium atoms reside on the positions 4*d*, rather than for models 1 and 2 with In atoms occupying the 8*h* sites (Figure 3). Because the scheme with the maximal number of heteroatomic contacts tends to give the lowest total energies for structures with disordered networks,[68] one would expect the model with the lowest homoatomic bond frequency to be the most favorable to compare to the experimental structure. A comparison of the total energies for the "$EuAu_5In$" models indicates that the lowest total energy is obtained for model 3, which is the scheme with the largest number of Au−In contacts per indium atom, and provides justification why indium prefers to occupy the 4*d* rather than the 8*h* sites.

Because preliminary calculations with varying correlation parameters (Figure S7, Supporting Information) indicated strong correlations for the Eu 4*f* states,[69−71] an effective on-site Coulomb interaction term (U_{eff} = 3 eV) was included as a correctional parameter to the Kohn−Sham Hamiltonian of the spin-polarized calculations. The total energy calculations on a ferromagnetic and an antiferromagnetic "$EuAu_4In_2$" model revealed an energy difference of 8.2 meV/cell between the antiferromagnetic and the lower lying ferromagnetic state, which tends to be preferred in fair agreement with the magnetic data.[72] The spin-polarized DOS curves of "$EuAu_4In_2$" (Figure S8, Supporting Information) do not superimpose, inferring a ferromagnetic state with a major difference for the Eu 4*f* states as the origin of a magnetic response.[72] The bands accounting for the Eu 4*f* AOs exhibit extremely small dispersions leading to sharp peaks at 4.22 and 11.72 eV in the spin-up and spin-down DOS curves, respectively. Such small dispersions are indicative of rather localized states playing a subordinate role in overall bonding and provide justification to treat the Eu 4*f* AOs as core-like states in the LMTO-based calculations.

Density of States. To provide insight into the electronic structures of the disordered tetragonal compositions $EuAu_{4+x}In_{2-x}$ (x = 0.8−1.0), which lie between those of the ordered "$EuAu_4In_2$" and "$EuAu_5In$", we followed up with an analysis of the DOS curves (Figure 4) for the "$EuAu_4In_2$" and the lowest energy "$EuAu_5In$" models. A comparison of the DOS curves for both models reveals significant contributions from the Au-d atomic orbitals (AOs), which mainly reside between −6.30 and −2.18 eV for "$EuAu_4In_2$" and between −6.57 and −2.01 eV for "$EuAu_5In$". The states near the Fermi level, E_F, originate primarily from the Au-d states with minor contributions from the Eu-d and In-p AOs, respectively. An analysis of the VASP-based DOS curves for a hypothetical model of "$Eu_5Au_{16}In_6$", which is derived from the orthorhombic structure of **III** through assignments of the major component indium on the disordered M sites (Wyckoff positions 8*f*, 8*f*, 8*f*), reveals alike tendencies (Figure S10, Supporting Information). In particular, the states below E_F arise mainly from the Au-d AOs (between −2.33 and 2.32 eV), whereas the states around the Fermi level stem mostly from the bands accounting for the Au-d AOs with minor shares from the Eu-d and In-p states, respectively. Because the refined composition of **III** has 41.4 valence electrons per formula unit (VEs/fu) and the composition of "$Eu_5Au_{16}In_6$" corresponds to 44 VEs/fu, it is rather inapt to evaluate stability tendencies for the $Eu_5Au_{16}(Au/In)_6$ structures based on the relative position of the Fermi level in "$Eu_5Au_{16}In_6$"; however, E_F in "$Eu_5Au_{16}In_6$" falls in a deep pseudogap, indicating an electronically favorable situation.

Notwithstanding that the general features are similar for "$EuAu_4In_2$" and "$EuAu_5In$", still, the models differ in both composition and valence electron counts (vec). The Fermi level in "$EuAu_4In_2$" (12 valence electrons) falls close to a local maximum in the DOS curve, while E_F in "$EuAu_5In$" (10 valence electrons) falls in a pseudogap that is generated in the DOS regions for vec of 9.9−10.6 VEs/fu. As the tetragonal structure

DOI: 10.1021/acs.inorgchem.5b00257
Inorg. Chem. 2015, 54, 8187−8196

Table 3. Distance and −ICOHP/Bond Ranges, Average −ICOHP/Bond, Cumulative −ICOHP/Cell, and Percentage Contributions of the Diverse Interactions in "$EuAu_4In_2$", "$EuAu_5In$-1", "$EuAu_5In$-2", "$EuAu_5In$-3", and "$EuAu_5In$-4"[a]

interaction	distance range [Å]	−ICOHP/bond range [eV/bond]	ave. −ICOHP/bond [eV/bond]	cum. −ICOHP	percentage
		"$EuAu_4In_2$"			
Au−Au	2.853−3.071	0.8351−0.7765	0.8058	12.8928	32.82
Au−Eu	3.187	0.3602	0.3602	2.8816	7.34
Au−In	3.021	0.6327	0.6327	20.2464	51.54
In−In	2.840	0.8155	0.8155	3.2620	8.30
		"$EuAu_5In$" model 1			
Au−Au	2.751−3.012	1.0496−0.4811	0.7586	27.3091	63.19
Au−Eu	3.103−3.194	0.3747−0.1915	0.2857	1.7144	3.97
Au−In	2.796−2.986	1.0148−0.6927	0.8317	13.3076	30.79
Eu−In	3.159	0.4418	0.4418	0.8836	2.05
		"$EuAu_5In$" model 2			
Au−Au	2.702−3.093	1.6429−0.5955	0.8740	32.3369	69.63
Au−Eu	2.988−3.200	0.5571−0.3650	0.4856	2.9134	6.27
Au−In	2.790−3.006	1.2100−0.5025	0.7503	10.5046	22.62
Eu−In	3.282	0.1580	0.1580	0.3160	0.68
In−In	3.117	0.3700	0.3700	0.3700	0.80
		"$EuAu_5In$" model 3			
Au−Au	2.844−3.013	1.0112−0.6365	0.7893	50.5130	57.05
Au−Eu	3.106−3.110	0.4051−0.3121	0.3600	5.7604	6.50
Au−In	2.794−2.983	0.9107−0.6484	0.8068	32.2714	36.45
		"$EuAu_5In$" model 4			
Au−Au	2.770−3.010	0.9405−0.5833	0.7436	49.0786	60.55
Au−Eu	3.111−3.125	0.3688−0.3113	0.3378	5.4044	6.67
Au−In	2.741−3.003	0.9884−0.6159	0.7062	25.4232	31.37
In−In	2.945	0.5740	0.5740	1.1480	1.41

[a]Tables compiling all distances, −ICOHP/bond, and their respective multiplicities are provided in the Tables S3−S6, Supporting Information.

II refines as $EuAu_{4.75}In_{1.25(2)}$, which corresponds to 10.5 VEs/fu, the Fermi level will be located near the higher part of the pseudogap in the "$EuAu_5In$" DOS. Likewise, E_F in $EuAu_{4.93}In_{1.07(2)}$ (10.1 VEs/fu) and $EuAu_{5.03}In_{0.97(2)}$ (9.9 VEs/fu) will occur near higher and lower parts of the pseudogap, respectively. This result alludes to a higher relevance of valence electron concentrations toward distributing gold and indium sites.

In summary, the total energy calculations point to a site preference of the 4*d* sites for the Au/In partitioning in the tetragonal structures. On the basis of an analysis of the DOS curves for both "$EuAu_4In_2$" and "$EuAu_5In$" valence electron concentrations appear to play a relevant role in these structures. Another important contribution that one would expect to influence the assignments of elements on intrinsic positions within one structure is the bond energy.[73] To analyze its impact on the tetragonal structure in more detail, we followed up with a (chemical) bonding analysis on the "$EuAu_4In_2$" and "$EuAu_5In$-3" models.

Bonding Analysis. Analysis of the −COHP curves (Figure 4) and their integrated values (Table 3) for both "$EuAu_4In_2$" and "$EuAu_5In$" model-3 indicates that significant bonding interactions are evident for the homoatomic M−M as well as the heteroatomic Au−In contacts. A direct comparison between the −ICOHP values of both systems cannot be made as the average electrostatic potential in each DFT-based calculations is scaled to an arbitrary "zero" energy;[74] however, projecting −ICOHP values weighted by bond frequencies as percentages to the total bonding capacities has been demonstrated to provide conclusive hints to the bonding differences between dissimilar structures.[53,54,75]

The Au−Au −ICOHP values range from 0.8351 to 0.7765 eV/bond for "$EuAu_4In_2$" and from 1.0112 to 0.6365 eV/bond for the more Au-rich composition and contribute 32.82% and 57.05% to the total bonding of the respective structures. Note that the percentage contribution of the Au−Au contacts is larger in "$EuAu_5In$" than in the more In-rich structure as a consequence of the higher Au−Au bond frequencies in "$EuAu_5In$". Because −ICOHP values tend to scale similarly to bond strength, generally, the magnitude of the −ICOHP values will decrease as the bond lengths increase. For example, the largest Au−Au −ICOHP value of the ordered "$EuAu_4In_2$" (0.8351 eV/bond) occurs for the separations (d = 2.853 Å) that enclose the squared bases of the Au_8 cages within the *ab* plane, while the Au−Au separations in the zigzag chains between these Au_4 squares are 3.071 Å and have an −ICOHP value of 0.7765 eV/bond. The homoatomic Au−Au interactions are optimized at −1.18 eV for "$EuAu_4In_2$" and at −1.58 eV for "$EuAu_5In$" and remain nonbonding until E_F. The strongly antibonding Au−Au interactions at around −3.26 eV for "$EuAu_4In_2$" and −3.05 eV for "$EuAu_5In$" stem from the repulsions of the Au-d orbitals, which are observed typically for gold-rich intermetallic compounds.[76]

The heteroatomic Au−In contacts are nonbonding around E_F (between −0.90 and 0.39 eV for "$EuAu_4In_2$" and between −0.44 and 1.55 eV for "$EuAu_5In$") and change to antibonding states at 0.39 eV for "$EuAu_4In_2$" and at 1.55 eV for "$EuAu_5In$". These interactions contribute 51.54% and 36.45% to the total bonding of "$EuAu_4In_2$" and "$EuAu_5In$-3", respectively. The difference in the percentage contributions of the Au−In contacts to the total bonding capacities originates from the dissimilar bond frequencies between "$EuAu_5In$" and "$EuAu_4In_2$", which has twice as many Au−In as Au−Au contacts.

DOI: 10.1021/acs.inorgchem.5b00257
Inorg. Chem. 2015, 54, 8187−8196

Another significant difference between the "$EuAu_4In_2$" and the "$EuAu_5In$" models is the absence of any close, homoatomic In−In contacts between the face-sharing $M@Au_8$ cages in the latter structure. These contacts (d = 2.840 Å) are evident for the ordered "$EuAu_4In_2$" and show bonding interactions with an −ICOHP value of 0.8155 eV/bond; in the more gold-rich model, however, the short Au−In separations (2.794 Å) exhibit strong bonding populations between the $M@Au_8$ cages.

A comparison of the Au−Au and Au−In −ICOHP values for the "$EuAu_4In_2$" and the lowest energy "$EuAu_5In$" models reveals that these values scale in the same range for the more Au-rich structure but show a significant difference in the ordered "$EuAu_4In_2$" (Table 3). As a consequence, there are strong Au−Au as well as Au−In bonding interactions in "$EuAu_5In$", whereas the −ICOHP values are much smaller for the heteroatomic than for the homoatomic contacts in the ordered "$EuAu_4In_2$". Although bond frequencies are a substantial factor in these structures and for their formations, this result also indicates the influence of the local symmetry and the intrinsic atomic arrangements. This impact comes even clearer from a comparison between "$EuAu_5In$" models 1 and 2. Even though model 1 has a higher Au−In bond frequency than model 2, this discrepancy is overcome by the higher amount of strong Au−Au interactions in 2, for which a lower total energy is evaluated rather than for model 1. This outcome suggests that the subtle interplay between Au−In bond frequencies and local atomic environments not only adjusts the site preferences for the Au/In partitioning but also controls the structural preferences for these compounds. The formally anionic networks of the diverse models encapsulate europium atoms, which reside in the centers of two face-sharing M_8 cages. The magnitudes of the M−Eu −ICOHP values are smaller than those for the Au−Au, Au−In, and In−In interactions, which is observed typically for rare-earth late-transition-metal intermetallic compounds.[68]

CONCLUSIONS

Exploration of the gold-rich regions for the Eu−Au−In system lead to the discovery of three ternary intermetallic compounds. $EuAu_{0.46}In_{1.54(2)}$ (**I**) can be derived from the binary $EuAu_2$ through partial indium occupation of the Au sites. Significant gold distributions on the indium sites are observed for the "$EuAu_4In_2$"-derived $EuAu_{4+x}In_{2-x}$ with x = 0.75(2) (**II**), 0.93(2), and 1.03(2). The mutual exchange of Au and In atoms for these structures while maintaining their host lattices substantiates the mutual exchangeabilities of Au and In but also points to certain electronical flexibilities for **I** and **II**. A combination of the structural elements of **I** and **II** was realized in $Eu_5Au_{17.29}In_{4.71(3)}$ (**III**), which adopts its own structure type. A topological analysis for the recently reported $Eu_5Au_{17.7}In_{4.3}$ and $Eu_5Au_{17.29}In_{4.71(3)}$ (**III**) reveals that these compounds formally represent one-dimensional intergrowths of the series $EuAu_2$−"$EuAu_{4+x}In_{2-x}$".

The electronic structure was examined for the $EuAu_{4+x}In_{2-x}$ compounds, which show the shortest repeat unit along (001) within the reported series. Electronic structure calculations on diverse "$EuAu_5In$" models indicated that there are clear site preferences of mixing indium on the 4*d* site rather than the 8*h* sites. From a topological analysis it becomes clear that this tendency arises from the attempt to optimize the frequency of the heteroatomic Au−In bonds, which is achieved through partial occupation of the 4*d* sites by indium. The positions of the Fermi level in the DOS of the "$EuAu_4In_2$" and the lowest energy "$EuAu_5In$" models reveal electronically favorable situations for the tetragonal structures but also suggest that valence electron concentrations are of higher relevance for their formations. On the basis of a chemical bonding analysis it is the subtle interplay between the heteroatomic bond frequencies and the approach to sustain strong local atomic contacts that ascertains the adaption of an intrinsic structure for this system.

ASSOCIATED CONTENT

Supporting Information

Tables of the atomic anisotropic displacement parameters for **I**, **II**, and **III**; simulated and measured PXRD patterns of **I**, **II**, and **III**; representations of the miscellaneous coordination environments in **II** and **III**; spin-polarized (VASP) and TB-LMTO-based DOS data for "$EuAu_4In_2$" and the lowest energy "$EuAu_5In$" model; distances, multiplicities and −ICOHP/bond values for selected interactions in "$EuAu_4In_2$" and all "$EuAu_5In$" models; DOS and projected DOS curves (VASP) of a hypothetical composition "$Eu_5Au_{16}In_6$"; crystallographic information on the ternary $EuAu_{0.46}In_{1.54(2)}$ (**I**), $EuAu_{4+x}In_{2-x}$ (x = 0.75(2) (**II**), 0.93(2), 1.03(2)) and $Eu_5Au_{17.29}In_{4.71(3)}$ (**III**) in cif form; The Supporting Information is available free of charge on the ACS Publications website at DOI: 10.1021/acs.inorgchem.5b00257.

AUTHOR INFORMATION

Corresponding Author

*E-mail: mudring@iastate.edu.

Notes

The authors declare no competing financial interest.

ACKNOWLEDGMENTS

This research was supported by the Office of Energy Efficiency and Renewable Energy, Advanced Manufacturing Office, the Office of the Basic Energy Sciences, Materials Sciences Division, U.S. DOE, and the Department of Materials Science and Engineering at Iowa State University. Ames Laboratory is operated for U.S. DOE by Iowa State University under contract No. DE-AC02-07CH11358. The authors also acknowledge the technical support of STOE & Cie (Dipl.-Ing. Jens Richter and Dr. Sascha Correll) with the acquisition of the PXRD patterns.

REFERENCES

(1) Corbett, J. D. *Inorg. Chem.* **2010**, *49*, 13−28.
(2) Pyykkö, P. *Chem. Rev.* **1988**, *88*, 563−594.
(3) Pyykkö, P. *Angew. Chem., Int. Ed.* **2004**, *43*, 4412−4456.
(4) Lin, Q.; Corbett, J. D. *Inorg. Chem.* **2009**, *48*, 5403−5411.
(5) Lin, Q.; Corbett, J. D. *Inorg. Chem.* **2011**, *50*, 11091−11098.
(6) Gupta, S.; Corbett, J. D. *Inorg. Chem.* **2012**, *51*, 2247−2253.
(7) Lin, Q.; Corbett, J. D. *J. Am. Chem. Soc.* **2007**, *129*, 6789−6797.
(8) Lin, Q.; Corbett, J. D. *Inorg. Chem.* **2008**, *47*, 7651−7659.
(9) Lin, Q.; Corbett, J. D. *Inorg. Chem.* **2010**, *49*, 10436−10444.
(10) Lin, Q.; Smetana, V.; Miller, G. J.; Corbett, J. D. *Inorg. Chem.* **2012**, *51*, 8882−8889.
(11) Smetana, V.; Lin, O.; Pratt, D. K.; Kreyssig, A.; Ramazanoglu, M.; Corbett, J. D.; Goldman, A. I.; Miller, G. J. *Angew. Chem., Int. Ed.* **2012**, *51*, 12699−12702.
(12) Lin, Q.; Vetter, J.; Corbett, J. D. *Inorg. Chem.* **2013**, *52*, 6603−6609.
(13) Mishra, T.; Lin, Q.; Corbett, J. D. *Inorg. Chem.* **2013**, *52*, 13623−13630.
(14) Palasyuk, A.; Grin, Y.; Miller, G. J. *J. Am. Chem. Soc.* **2014**, *136*, 3108−3117.

DOI: 10.1021/acs.inorgchem.5b00257
Inorg. Chem. 2015, 54, 8187−8196

(15) Smetana, V.; Steinberg, S.; Card, N.; Mudring, A.-V.; Miller, G. J. *Inorg. Chem.* **2015**, *54*, 1010−1018.
(16) Lin, Q.; Mishra, T.; Corbett, J. D. *J. Am. Chem. Soc.* **2013**, *135*, 11023−11031.
(17) Gerke, B.; Hoffmann, R.-D.; Pöttgen, R. *Z. Anorg. Allg. Chem.* **2013**, *639*, 2444−2449.
(18) Gerke, B.; Pöttgen, R. *Z. Naturforsch.* **2014**, *69b*, 121−124.
(19) Bruzzone, G. *Atti Accad. Naz. Lincei, Cl. Sci. Fis., Mater. Nat. Rend.* **1970**, *48*, 235−241.
(20) Zachwieja, U. *J. Alloys Compd.* **1996**, *235*, 12−14.
(21) Iandelli, A.; Palenzona, A. *J. Less-Common Met.* **1968**, *15*, 273−284.
(22) Gerke, B.; Niehaus, O.; Hoffmann, R.-D.; Pöttgen, R. *Z. Anorg. Allg. Chem.* **2013**, *639*, 2575−2580.
(23) Mishra, T.; Lin, Q.; Corbett, J. D. *J. Solid State Chem.* **2014**, *218*, 103−108.
(24) Fornasini, M. L.; Palenzona, A. *J. Less-Common Met.* **1976**, *45*, 137−141.
(25) Muts, I.; Matar, S. F.; Rodewald, U. C.; Zaremba, V. I.; Pöttgen, R. *Z. Naturforsch., B: J. Chem. Sci.* **2011**, *66*, 993−999.
(26) Tappe, F.; Matar, S. F.; Schwickert, C.; Winter, F.; Gerke, B.; Pöttgen, R. *Monatsh. Chem.* **2013**, *144*, 751−760.
(27) Fornasini, M. L.; Mazzone, D.; Provino, A.; Michetti, M.; Paudyal, D.; Gschneidner, K.; Manfrinetti, P. *Intermetallics* **2014**, *53*, 169−176.
(28) Provino, A.; Steinberg, S.; Smetana, V.; Kulkarni, R.; Dhar, S. K.; Manfrinetti, P.; Mudring, A.-V. *J. Mater. Chem. C* **2015**, DOI: 10.1039/C5TC00884K.
(29) Morita, Y.; Tsai, A.-P. *Jpn. J. Appl. Phys.* **2008**, *47*, 7975−7979.
(30) Hoffmann, R. D.; Pöttgen, R.; Rosenhahn, C.; Mosel, B. D.; Künnen, B.; Kotzyba, G. *J. Solid State Chem.* **1999**, *145*, 283−290.
(31) Muts, I. R.; Schappacher, F. M.; Hermes, W.; Zaremba, V. I.; Pöttgen, R. *J. Solid State Chem.* **2007**, *180*, 2202−2208.
(32) Sarkar, S.; Gutmann, M. J.; Peter, S. C. *Cryst. Growth Des.* **2013**, *13*, 4285−4294.
(33) Muts, I.; Rodewald, U. C.; Zaremba, V. I.; Pavlosyuk, O.; Pöttgen, R. *Z. Naturforsch., B: J. Chem. Sci.* **2012**, *67*, 107−112.
(34) *WinXPOW*, 3.0.2.1 ed.; STOE & Cie GmbH: Darmstadt, Germany, 2011.
(35) Pöttgen, R. *J. Mater. Chem.* **1996**, *6*, 63−67.
(36) *SMART*; Bruker AXS, Inc.: Madison, WI, 1996.
(37) Blessing, R. *Acta Crystallogr., Sect. A: Found. Crystallogr.* **1995**, *51*, 33−38.
(38) *SHELXTL*; Bruker AXS Inc.: Madison, WI, 2000.
(39) Sheldrick, G. M. *Acta Crystallogr., Sect. A: Found. Crystallogr.* **2008**, *64*, 112−122.
(40) Spek, A. L. *Acta Crystallogr., Sect. D: Biol. Crystallogr.* **2009**, *65*, 148−155.
(41) Blöchl, P. E. *Phys. Rev. B: Condens. Matter Mater. Phys.* **1994**, *50*, 17953−17979.
(42) Kresse, G.; Marsman, M.; Furthmüller, J. *Vienna Ab initio Simulation Package (VASP) VASP, the user Guide*; Universität Wien: Wien, Austria, 2010.
(43) Kresse, G.; Furthmüller, J. *Comput. Mater. Sci.* **1996**, *6*, 15−50.
(44) Kresse, G.; Furthmüller, J. *Phys. Rev. B: Condens. Matter Mater. Phys.* **1996**, *54*, 11169−11186.
(45) Kresse, G.; Hafner, J. *Phys. Rev. B: Condens. Matter Mater. Phys.* **1993**, *47*, 558−561.
(46) Kresse, G.; Joubert, D. *Phys. Rev. B: Condens. Matter Mater. Phys.* **1999**, *59*, 1758−1775.
(47) Perdew, J. P.; Burke, K.; Ernzenhof, M. *Phys. Rev. Lett.* **1996**, *77*, 3865−3868.
(48) Tank, R.; Jepsen, O.; Burkhardt, A.; Andersen, O. K. *TB-LMTO-ASA Program*, version 4.7; Max-Planck-Institut für Festkörperforschung: Stuttgart, Germany, 1994.
(49) Andersen, O. K.; Jepsen, O. *Phys. Rev. Lett.* **1984**, *53*, 2571−2574.
(50) Dronskowski, R.; Blöchl, P. E. *J. Phys. Chem.* **1993**, *97*, 8617−8624.
(51) Lambrecht, W. R. L.; Andersen, O. K. *Phys. Rev. B: Condens. Matter Mater. Phys.* **1986**, *34*, 2439−2449.
(52) Chai, P.; Corbett, J. D. *Inorg. Chem.* **2012**, *51*, 3548−3556.
(53) Gupta, S.; Meyer, G.; Corbett, J. D. *Inorg. Chem.* **2010**, *49*, 9949−9957.
(54) Steinberg, S.; Bell, T.; Meyer, G. *Inorg. Chem.* **2015**, *54*, 1026−1037.
(55) Blöchl, P. E.; Jepsen, O.; Andersen, O. K. *Phys. Rev. B: Condens. Matter Mater. Phys.* **1994**, *49*, 16223−16233.
(56) Larson, A. C.; Cromer, D. T. *Acta Crystallogr.* **1961**, *14*, 73−74.
(57) Iandelli, A. *Z. Anorg. Allg. Chem.* **1964**, *330*, 221−232.
(58) Dai, J.-C.; Corbett, J. D. *Inorg. Chem.* **2006**, *45*, 2104−2111.
(59) Pöttgen, R.; Kotzyba, G.; Görlich, E. A.; Latka, K.; Dronskowski, R. *J. Solid State Chem.* **1998**, *141*, 352−364.
(60) Wendorff, M.; Röhr, C. *Z. Anorg. Allg. Chem.* **2005**, *631*, 338−349.
(61) Manfrinetti, P.; Fornasini, M. L.; Mazzone, D.; Dhar, S. K.; Kulkarni, R. *J. Alloys Compd.* **2004**, *379*, 64−71.
(62) Solokha, P.; DeNegri, S.; Pavlyuk, V.; Saccone, A.; Fadda, G. *Eur. J. Inorg. Chem.* **2012**, *2012*, 4811−4821.
(63) Verbovytskyy, Y.; Gonçalves, A. P. *Solid State Sci.* **2015**, *40*, 84−91.
(64) Grin, Y. N. In *Modern Perspectives in Inorganic Crystal Chemistry*; Parthé, E., Ed.; Kluwer Academic Publishers: Dordrecht, The Netherlands, 1992; pp 77−95.
(65) Han, M.-K.; Miller, G. J. *Inorg. Chem.* **2008**, *47*, 515−528.
(66) You, T.-S.; Miller, G. J. *Inorg. Chem.* **2009**, *48*, 6391−6401.
(67) Wang, F.; Pearson, K. N.; Strazheim, W. E.; Miller, G. J. *Chem. Mater.* **2010**, *22*, 1798−1806.
(68) Wang, F.; Pearson, K. N.; Miller, G. J. *Chem. Mater.* **2009**, *21*, 230−236.
(69) Setyawan, W.; Curtarolo, S. *Comput. Mater. Sci.* **2010**, *49*, 299−312.
(70) Ranjan, R.; Nabi, H. S.; Pentcheva, R. *J. Phys.: Condens. Matter* **2007**, *19*, 406217.
(71) Rocquefelte, X.; Gautier, R.; Halet, J.-F.; Müllmann, R.; Rosenhahn, C.; Mosel, B. D.; Kotzyba, G.; Pöttgen, R. *J. Solid State Chem.* **2007**, *180*, 533−540.
(72) Bigun, I.; Steinberg, S.; Smetana, V.; Mudryk, Y.; Pecharsky, V.; Mudring, A.-V. *Manuscript in preparation*.
(73) Miller, G. J. *Eur. J. Inorg. Chem.* **1998**, *1998*, 523−536.
(74) Börnsen, N.; Meyer, B.; Grotheer, O.; Fähnle, M. *J. Phys.: Condens. Matter* **1999**, *11*, L287−L293.
(75) Steinberg, S.; Brgoch, J.; Miller, G. J.; Meyer, G. *Inorg. Chem.* **2012**, *51*, 11356−11364.
(76) Köhler, J.; Whangbo, M.-H. *Solid State Sci.* **2008**, *10*, 444−449.

DOI: 10.1021/acs.inorgchem.5b00257
Inorg. Chem. 2015, 54, 8187−8196